European Journal of Radiology 172 (2024) 111359

Contents lists available at ScienceDirect

European Journal of Radiology

journal homepage: www.elsevier.com/locate/ejrad

Comparison of the accuracy of commercial two-point and multi-echo Dixon MRI for quantification of fat in liver, paravertebral muscles, and vertebral bone marrow

Tobias Haueise [a,b], Fritz Schick [a,b,c], Norbert Stefan [b,c,d], Jürgen Machann [a,b,c,*]

[a] Institute for Diabetes Research and Metabolic Diseases, Helmholtz Munich at the University of Tübingen, Tübingen, Germany
[b] German Center for Diabetes Research (DZD), Tübingen, Germany
[c] Section on Experimental Radiology, Department of Diagnostic and Interventional Radiology, University Hospital Tübingen, Tübingen, Germany
[d] Department of Diabetology, Endocrinology and Nephrology, University Hospital Tübingen, Tübingen, Germany

ARTICLE INFO

Keywords:
Magnetic resonance imaging
Dixon MRI
Vertebral bone marrow
Fat fraction estimation

ABSTRACT

Purpose: Excess fat accumulation contributes significantly to metabolic dysfunction and diseases. This study aims to systematically compare the accuracy of commercially available Dixon techniques for quantification of fat fraction in liver, skeletal musculature, and vertebral bone marrow (BM) of healthy individuals, investigating biases and sex-specific influences.

Method: 100 healthy White individuals (50 women) underwent abdominal MRI using two-point and multi-echo Dixon sequences. Fat fraction (FF), proton density fat fraction (PDFF) and T2* values were calculated for liver, paravertebral muscles (PVM) and vertebral BM (Th8–L5). Agreement and systematic deviations were assessed using linear correlation and Bland-Altman plots.

Results: High correlations between FF and PDFF were observed in liver ($r = 0.98$ for women; $r = 0.96$ for men), PVM ($r = 0.92$ for women; $r = 0.93$ for men) and BM ($r = 0.97$ for women; $r = 0.95$ for men). Relative deviations between FF and PDFF in liver (18.92 % for women; 13.32 % for men) and PVM (1.96 % for women; 11.62 % for men) were not significant. Relative deviations in BM were significant (38.13 % for women; 27.62 % for men). Bias correction using linear models reduced discrepancies. T2* times were significantly shorter in BM (8.72 ms for women; 7.26 ms for men) compared to PVM (13.45 ms for women; 13.62 ms for men) and liver (29.47 ms for women; 26.35 ms for men).

Conclusion: While no significant differences were observed for liver and PVM, systematic errors in BM FF estimation using two-point Dixon imaging were observed. These discrepancies – mainly resulting from organ-specific T2* times – have to be considered when applying two-point Dixon approaches for assessment of fat content. As suitable correction tools, linear models could provide added value in large-scale epidemiological cohort studies. Sex-specific differences in T2* should be considered.

1. Introduction

Excess accumulation of ectopic fat within various anatomical compartments in the human body has been recognized as a significant indicator of metabolic dysfunction, insulin resistance, and various diseases, such as type-2 diabetes, atherosclerosis, multiple myeloma or osteoporosis [1–3]. Non-invasive and reliable quantification of fat accumulation within specific tissues, such as bone marrow (BM) in vertebral bodies, musculature, and liver, is pivotal for understanding their impact on health and disease [4–7].

Magnetic resonance imaging (MRI) and volume localized spectroscopy (MRS) have emerged as important tools in this endeavor. Modern MRI techniques provide non-invasive assessment of macroscopic fat distribution [8,9] as well as ectopic fat accumulation within organs and tissues [10–12] with high spatial resolution. Among the various MRI methods available, Dixon-type imaging has gained substantial attention for its ability to distinguish between water and fat content within tissues [13] even in regions with inhomogeneous magnetic field distribution. Further, Dixon MRI can be used to measure fat fraction (FF) at the voxel level.

* Corresponding author at: Hoppe-Seyler-Str. 3, 72076 Tübingen, Germany.
E-mail address: juergen.machann@med.uni-tuebingen.de (J. Machann).

https://doi.org/10.1016/j.ejrad.2024.111359
Received 1 February 2024; Accepted 3 February 2024
Available online 5 February 2024

However, the choice of Dixon MRI sequence and the methods employed for postprocessing of recorded imaging data can significantly affect the accuracy and reliability of FF measurements as reflected, e. g., in the compromise between acquisition time, image resolution, and accuracy.

In contrast to two-point Dixon imaging, which acquires images at two echo times (in-phase/opposed-phase) enabling calculation of fat-selective images, but requires an internal reference for (magnitude-based) FF estimation, multi-echo Dixon imaging allows for absolute quantification of fat fraction defined as proton density fat fraction (PDFF). Commercially available multi-echo Dixon sequences have been optimized for PDFF quantification in the liver by implementation of T1-insensitive acquisition, T2*-correction, and consideration of the spectral complexity of fat [14]. For this purpose, they are validated in terms of linearity, precision and reproducibility in multisite, multivendor phantom studies [15–17] and *in vivo* [18–20]. As reviewed by Starekova et al., widespread application of imaging-based PDFF assessment justify the assumption of this as a reference [20].

PDFF quantification is also of interest for other organs and tissues, e. g. paravertebral muscles (PVM) or vertebral bone marrow (BM) [21,22]. However, lipids in red BM in vertebral bodies are metabolically distinct from other fat depots [23] and their assessment is confounded, as paramagnetic hematopoietic cells and the presence of trabecular structures influence the microscopic magnetic field distribution inside the vertebral bodies [24]. Additionally, water and lipid signals in red BM often show similar spectral signal intensities [25]. BM fat is subject of several studies analyzing its associations, e. g., with body composition, osteoporosis or degeneration of intervertebral discs [26–28]. Therefore, precise quantification of vertebral BM fat content using Dixon-based MR sequences is necessary.

Aim of the present study is the systematic comparison of two-point Dixon imaging with multi-echo Dixon imaging as a reference in a cohort of healthy individuals to investigate and assess biases of fat quantification in liver, PVM, and BM of thoracic and lumbar vertebral bodies.

2. Materials and methods

In this analysis, data from 100 healthy volunteers who self-reported as White individuals (50 women, sex defined based on self-report) participating in ongoing studies involving metabolic imaging, which were related to the Tübingen Diabetes Family Study [6], in Tübingen, Germany, were included. All individual studies were approved by the Ethics Committee of the University Hospital Tübingen and written informed consent was obtained from all participants prior to participation.

MR examinations were performed on a 3 T whole-body scanner (Magnetom Vida, Siemens Healthcare, Erlangen, Germany). Subjects were positioned head first in supine position on a 24-channel table-integrated spine-array coil. For homogeneous coverage of the body trunk, two 18-channel body-array coils were placed on chest and lower abdomen. A 3D volumetric interpolated breath-hold examination (VIBE) two-point Dixon sequence (regular product functionality) and a multi-echo Dixon VIBE sequence (LiverLab option) using six echoes were applied in three axial slabs covering the trunk. Sequence parameters of both acquisitions are summarized in Table 1.

Two-point FF maps from two-point measurement were calculated offline using fat-selective (F) and water-selective (W) images by voxel-wise application of the formula $FF = F/(F + W)$. Multi-echo PDFF maps were generated inline on the console of the scanner by the vendor's algorithm, correcting for microscopic magnetic field inhomogeneities by modeling of an effective transverse relaxation time (T2*) and spectrally complex fat dephasing [14].

For objective measurements without manual and subjective placement of single ROIs, fat quantification was performed using automatically generated segmentation masks of liver [29], ten vertebral bodies of the thoracic and lumbar spine (Th8–L5) [30], and PVM (right/left erector spinae and psoas major muscles) [31] by averaging voxel fat fraction map values inside each segmented fat compartment. By applying two-dimensional erosion in the axial plane using a 3x3 matrix as structuring element, edge pixels were excluded. T2* was measured from the corresponding maps using the mean value over the same generated segmentation masks.

Table 1
Sequence parameters. MRI acquisition parameters as applied on a whole-body scanner (Magnetom Vida, Siemens Healthcare, Erlangen, Germany).

	Two-point Dixon	Multi-echo Dixon
Matrix size	320x161	160x104
Field of view / mm x mm	550x395	380x313
In-plane resolution / mm x mm	1.4 x 1.4	1.2 x 1.2
Slice thickness / mm	3	3
Partitions per slab	80	80
TE / ms	1.23, 2.46	1.09, 2.46, 3.69, 4.92, 6.15, 7.38
TR / ms	4.36	13
Flip angle / Degree	9	4
Bandwidth / Hz/Pixel	1042	1078
TA / s	12.6	16.2

TE: Echo times TR: Repetition time TA: Acquisition time.

All data are reported as mean (SD) unless stated otherwise. Linear correlation analysis and Bland-Altman plots were used to quantify and visualize the bias and agreement between FF and PDFF. Differences are expressed as percentages ([FF-PDFF]/mean %). Deviations from FF compared to PDFF are reported as "relative" percentages ([FF-PDFF]/PDFF %) unless stated otherwise. Welch's *t*-test was selected to test for statistically significant differences between women and men. Holm-Bonferroni method was applied to correct p-values for multiple testing when comparing vertebral bodies. $p < 0.05$ was considered statistically significant. All statistical analyses were performed in Python 3.8 using SciPy 1.8.0 and statsmodels 0.13.2.

3. Results

Imaging errors (e. g. partial fat–water swaps in the liver) and errors during computation of PDFF led to the exclusion of five participants. One participant was excluded due to a potentially pathologically low PDFF in BM, not fulfilling the assumption of a "healthy volunteer". The analyzed study population is characterized in Table 2. An exemplary coronal PDFF map is shown in Fig. 1.

FF estimation showed high correlation with PDFF in the liver ($r = 0.98$, for women; $r = 0.96$, for men, see Fig. 2a), in PVM ($r = 0.92$, for women; $r = 0.93$, for men, see Fig. 2b) and BM averaged along the spine (including vertebral bodies Th8–L5; $r = 0.97$, for women; $r = 0.95$, for men, see Fig. 2c). Correlation strength was significantly different for men and women ($p < 0.05$). In the liver, fitted sex-specific linear

Table 2
Study population. Anthropometric data of the study population. Range of the values is presented in square brackets.

	Women	Men
N	47	47
Age / years	42.7 (14.8) [20–67]	46.1 (15.9) [23–76]
Height /cm	167.9 (7.1) [148.5–185.0]	180.9 (8.2)*** [163.0–198.2]
Weight / kg	75.7 (19.1) [46.2–112.0]	87.5 (16.0)** [59.0–144.6]
BMI / kg/m^2	27.1 (7.5) [15.5–40.4]	26.8 (4.6) [18.9–37.9]

Sex differences: $^{**}p < 0.01$, $^{***}p < 0.001$.

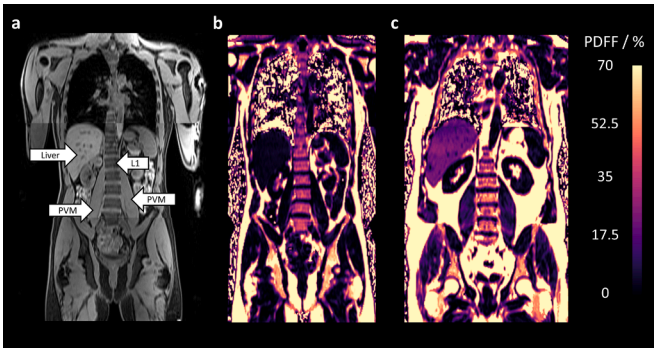

Fig. 1. Exemplary imaging data. Water-selective image slice from two-point acquisition (**a**) highlighting analyzed regions-of-interest and corresponding PDFF map (**b**) of a 28-year old man (BMI 22.3 kg/m^2, 3.50 % liver PDFF, 3.71 % muscle PDFF, 33.90 % mean bone marrow PDFF). (**c**) Coronal PDFF map of a 58-year old man with high liver and muscle PDFF (BMI 35.2 kg/m^2, 20.4 % liver PDFF, 8.64 % muscle PDFF, 39.27 % mean bone marrow PDFF).

regression models predicting PDFF from FF along with 95 % CI of regression parameters were: PDFF = 0.83 [0.79 to 0.88] x FF + 0.15 [−0.17 to 0.48] for women; PDFF = 0.83 [0.76 to 0.90] x FF + 0.61 [−0.07 to 1.28] for men. In PVM, the fitted models were: PDFF = 1.38 [1.20 to 1.56] x FF − 2.34 [−3.49 to −1.20] for women; PDFF = 1.29 [1.14 to 1.44] x FF − 2.23 [−3.20 to −1.26] for men. In BM, the fitted models were: PDFF = 0.86 [0.85 to 0.88] x FF − 5.89 [−6.82 to −4.97] for women; PDFF = 0.81 [0.79 to 0.84] x FF − 1.19 [−2.32 to −0.05] for men.

As detailed in Table 3, differences between FF and PDFF in liver and PVM are not significant for both sexes ($p = 0.41$ and $p = 0.79$ for women; $p = 0.68$ and $p = 0.25$ for men, respectively). Liver FF was increased compared to corresponding PDFF by 18.92 % in women and by 13.32 % in men. In PVM, FF was increased by 1.96 % in women and by 11.62 % in men. In contrast, FF in vertebral BM was significantly increased compared to PDFF by an average over all analyzed vertebral bodies of 38.13 % in women (ranging from 34.98 % in L5 to 41.00 % in Th9) and by an average of 27.62 % in men (ranging from 25.65 % in Th9 to 29.73 % in Th12). Across both sexes, bias in liver FF was 12.21 %, 5.27 % in PVM and 27.78 % in BM (see Fig. 3). With increasing mean fat content, bias in PVM and BM decreased (see Fig. 3b and 3c). In PVM, this even led to a shift from overestimation to underestimation of PDFF (see Fig. 3b). For mean fat fractions above 5 %, bias in the liver was almost constant (see Fig. 3a).

Considering FF estimation alone, apparently significant differences were found between different vertebral bodies, which could not be confirmed in PDFF quantification. In women and men, significant differences between PDFF in lower lumbar vertebrae (L4 and L5) and the mid thoracic spine (Th8–Th10) were found. In men, L1 and L2 were also significantly different from Th8–Th10 (see Fig. 4).

As measured from multi-echo Dixon, differences in T2* times between different vertebral bodies were not significant for women and men. Mean T2* in BM and liver were significantly higher for women compared to men (8.72 ms for women, 7.26 ms for men, $p < 0.001$, in BM; 29.47 ms for women, 26.35 ms for men, $p < 0.05$, in the liver; see Table 4). Sex differences in PVM were not significant ($p = 0.74$). For both sexes, mean T2* in BM was significantly lower compared to PVM and liver ($p < 0.001$).

Derived sex-specific linear regression models for BM PDFF (see Fig. 2c) can be used to correct for the bias in FF estimation. After application, FF overestimation was reduced to 0.04 % along the spine and across both sexes (see Fig. 5b). Additionally, apparently significant differences between FF and PDFF in the vertebral bodies, cannot be removed by linear correction.

4. Discussion

This study systematically compared two-point Dixon and a multi-echo Dixon sequences for the quantification of fat fraction in liver, paravertebral muscles (PVM) and bone marrow (BM) in vertebral bodies of the thoracic and lumbar spine (Th8–L5) in healthy subjects.

Table 3
Measured fat fractions. Fat fraction measurements (in "absolute" %) in liver, paravertebral muscles and vertebral bone marrow (Th8–L5) using a two-point and multi-echo Dixon sequence.

	Women		Men	
In %	PDFF	FF	PDFF	FF
Liver	4.73 (4.00)	5.48 (4.72)	6.29 (5.96)	6.84 (6.91)
PVM	6.55 (1.93)	6.46 (1.30)	5.90 (1.83)	6.28 (1.32)
Th8	30.51 (10.61)	41.92 (12.02)$^{+++}$	33.62 (7.79)	42.49 (9.69)$^{+++}$
Th9	29.66 (9.24)	41.02 (10.87)$^{+++}$	33.79 (7.80)	42.30 (9.63)$^{+++}$
Th10	31.03 (9.99)	42.10 (11.66)$^{+++}$	34.42 (7.64)	43.26 (9.98)$^{+++}$
Th11	32.05 (10.08)	43.71 (12.52)$^{+++}$	36.10 (8.09)	45.84 (9.72)$^{+++}$
Th12	34.49 (11.65)	47.02 (12.81)$^{+++}$	38.06 (8.44)	48.95 (9.39)$^{+++}$
L1	35.20 (10.99)	48.23 (12.25)$^{+++}$	38.88 (8.45)	49.81 (9.24)$^{+++}$
L2	36.39 (11.24)	49.08 (12.16)$^{+++}$	40.18 (8.40)	51.19 (9.22)$^{+++}$
L3	38.11 (11.66)	50.91 (12.56)$^{+++}$	41.22 (8.62)	52.18 (9.27)$^{+++}$
L4	39.54 (12.33)	52.32 (13.19)$^{+++}$	41.35 (8.71)	52.78 (9.88)$^{+++}$
L5	40.39 (13.18)	53.46 (14.28)$^{+++}$	43.54 (8.94)	54.61 (9.65)$^{+++}$

Intra-sex sequence differences: $^{+++}p < 0.001$; PVM: paravertebral muscles, PDFF: proton density fat fraction, FF: fat fraction from two-point Dixon

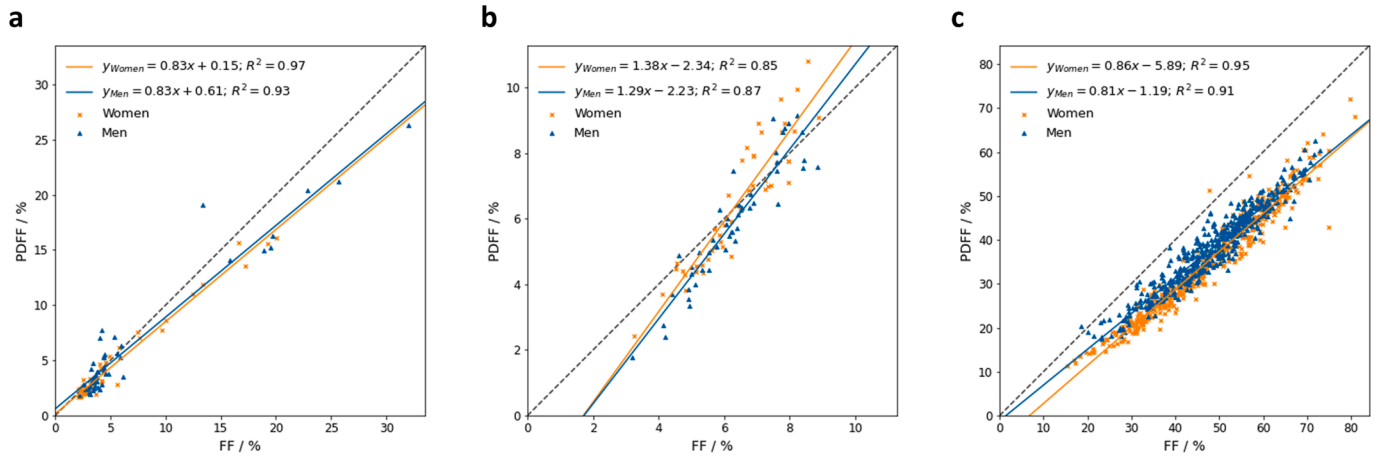

Fig. 2. Comparison of FF and PDFF. Comparison of two-point FF estimation with multi-echo PDFF quantification in the liver (**a**), paravertebral muscles (**b**) and in vertebral bone marrow (Th8–L5) (**c**).

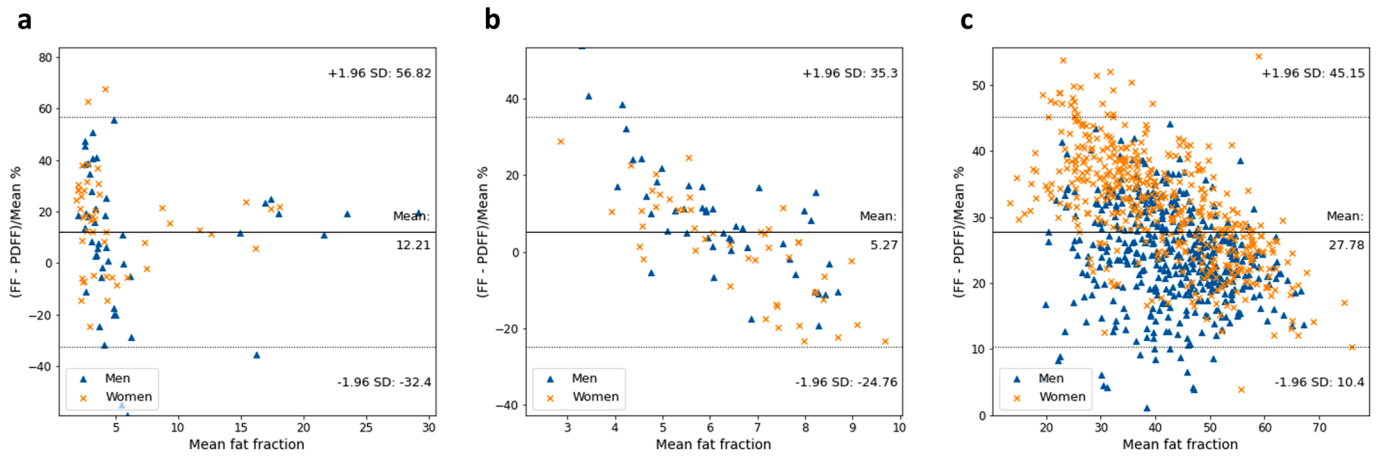

Fig. 3. Agreement of FF and PDFF. Bland-Altman plot comparing relative deviations between two-point FF estimation with multi-echo PDFF quantification in the liver (**a**), paravertebral muscles (**b**) and in vertebral bone marrow (Th8–L5) (**c**).

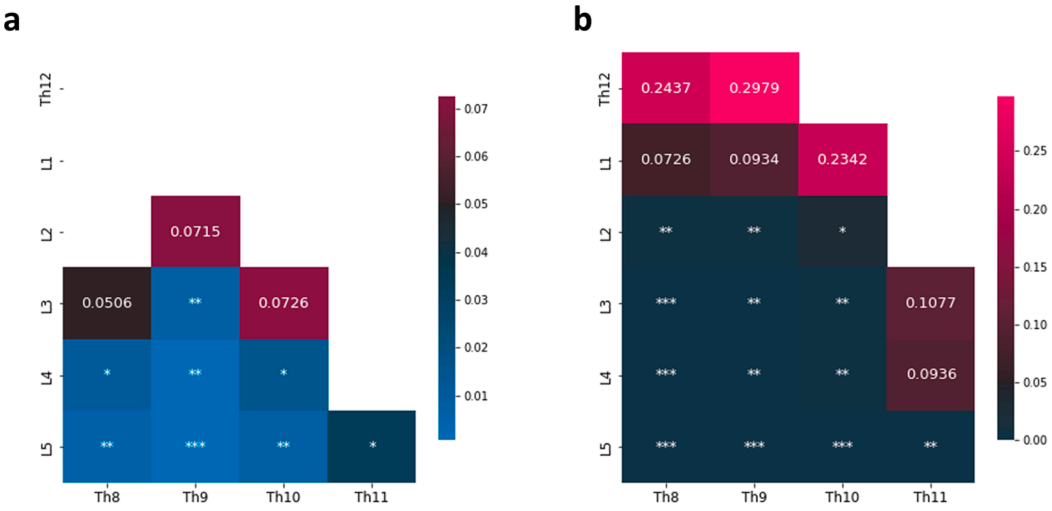

Fig. 4. Apparently significant differences. Holm-Bonferroni corrected *p*-values of apparently significant differences between FF and PDFF in vertebral bodies ($^{*}p < 0.05$, $^{**}p < 0.01$, $^{***}p < 0.001$) in women (**a**) and men (**b**).

Table 4
T2*. Mean T2* times for analyzed fat compartments as obtained from automatic calculation during image reconstruction using multi-echo Dixon sequence.

In ms	Women	Men
Liver	29.47 (5.22)	26.35 (8.51)*
PVM	13.45 (2.38)	13.62 (2.43)
Th8	8.99 (1.52)	7.59 (1.50)***
Th9	8.95 (1.47)	7.58 (1.49)***
Th10	8.69 (1.30)	7.11 (1.47)***
Th11	8.46 (1.24)	7.17 (1.47)***
Th12	8.78 (1.33)	7.26 (1.45)***
L1	8.76 (1.12)	7.39 (1.38)***
L2	8.59 (1.01)	7.25 (1.39)***
L3	8.56 (1.00)	7.12 (1.27)***
L4	8.50 (0.99)	7.11 (1.23)***
L5	8.90 (2.44)	7.02 (1.20)***

Sex differences: $^{*}p < 0.05$, $^{***}p < 0.001$; PVM: paravertebral muscles.

Significant differences in the estimation of vertebral BM fat fraction, despite very high correlation, were found. Using sex-specific linear regression models (as shown in Fig. 2c) for the correction of two-point FF in BM, bias between the corrected FF values and the multi-echo PDFF values can be removed (see Fig. 5). However, apparently significant differences between FF of single vertebral bodies could not be removed in the present analysis. This suggests that multi-echo measurements seem to be more suitable for in-depth analysis of BM fat beyond mere fat quantification.

Deviations between "confounder-corrected" fat quantification based on multi-echo Dixon PDFF maps and simple estimations from two echoes can stem from multiple sources: First, differences in T1 for the water and fat components of different tissues. As reviewed by Bojorquez et al., at 3 T, T1 in the liver ranges from 725 to 809 ms, lies between 898 and 1420 ms in muscle and is with a range between 106 and 586 ms notably shorter in BM [32]. More specifically, de Bazelaire et al. reported 809 ms for liver, 898 ms for paravertebral muscles and 586 ms for bone marrow in L4 using an inversion-recovery method and multiple spin-echo technique [33]). Second, different fat-to-water ratios can lead to under- or overestimation [34], and will scale with the flip angle of the acquisition, as well as with flip angle heterogeneity, especially in vertebral bodies due to trabecular structures. Although the applied two-point sequence is characterized by stronger T1-weighting compared to the multi-echo sequence, a resulting T1-effect is assumed to be less pronounced in BM due to shorter T1 (see above). Third, when not accounted for, the spectral complexity of fat will also cause the deviations to be dependent on the choice of echo times. T2* relaxation will reduce the signal intensity of later echoes, so the order of in-phase and opposed-phase echoes will become important. Especially inside the vertebral bodies,

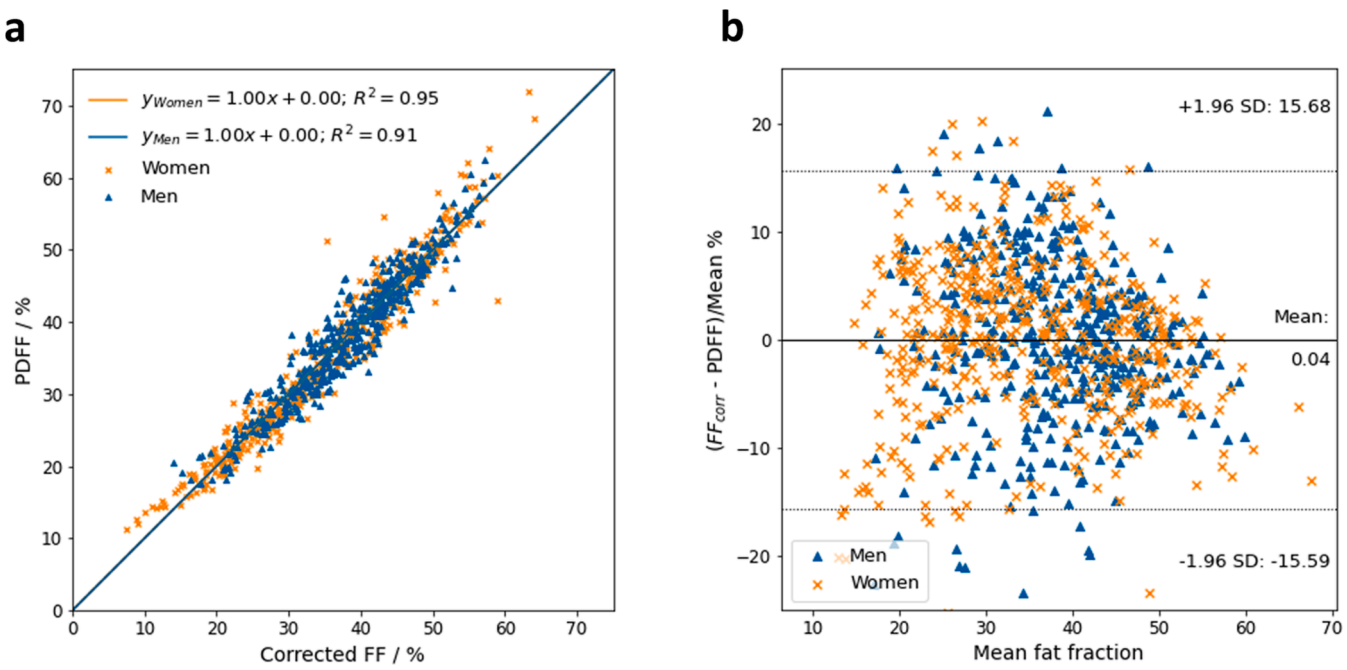

Fig. 5. Comparison and agreement of corrected FF. Comparison (**a**) and Bland-Altman plot (**b**) of corrected two-point FF and multi-echo PDFF in vertebral bone marrow (Th8–L5) as obtained from sex-specific linear regression models y = 0.86x-5.89 for women and y = 0.81x-1.19 for men.

heterogeneous trabecular structures and paramagnetic hematopoietic cells directly affect T2*.

This study has some limitations. First, only two different MR sequences from one manufacturer are considered. However, as images are taken from ongoing studies and the sequences used are also applied in large epidemiological cohort studies like KORA or *NAKO Gesundheitsstudie* [35,36], the results are of interest for a wide range of applications, as multiple studies investigated MRI-assessed BM fat and its correlation to body fat distribution, physical activity, as well as metabolic diseases, osteoporosis or its characterization after transplantation [3,26,28,37–40]. In other large-scale epidemiological cohort studies, such as UK Biobank, two-point Dixon imaging is also applied [41]. Furthermore, the underlying problem is in principle independent of sequence parameters and manufacturers: two-point measurements always have the problem of limited potential for confounder correction. However, no quantitative statement can be made about other manufacturers, but the results of the study can provide a qualitative indication of the expected level of error and the need for correction. Particularly in the liver, T2* can shorten dramatically in disease (iron overload) [42]. Thus, a fixed-factor T2* correction in two-point Dixon reconstruction may not be feasible. Second, the consideration of multi-echo Dixon PDFF as a baseline for comparison is not a true gold standard, as, inter alia, the adjustment for T2* correction is not ideal due to generally shorter effective relaxation times and owing to potential differences in the spectral composition of fat in bone marrow, which is calibrated for the liver [25]. Third, significant sex differences in FF inside the vertebral bodies, as well as in T2*, are not accounted for in two-point reconstruction. Finally, it has to be mentioned that the findings are limited to healthy subjects and might differ in patients with chronic liver disease [20], patients with neuromuscular disorders (muscular dystrophies) [21], or patients with hematological diseases undergoing cytostatic treatment or radiotherapy [40,43], where micro- and macroscopic alterations of the respective tissue have to be considered.

5. Conclusion

This study suggests that using two-point Dixon imaging for quantification of fat fraction in vertebral bone marrow reveals higher systematic errors compared to liver and/or muscle. Due to the high correlation between two-point and multi-echo FF estimation, simple tools such as linear models could be used to compensate for these systematic errors, as long as the acquisition parameters remain unchanged, when analyzed in large-scale epidemiological studies. Significant sex differences in T2* inside the vertebral bodies suggest the need for sex-specific reconstructions.

Funding

This work was supported in part by a grant of the German Research Foundation [428224476/SPP2177]; and in part by a grant from the Federal Ministry of Education and Research (BMBF) to the German Center for Diabetes Research (DZD e.V.) [01GI0925].

CRediT authorship contribution statement

Tobias Haueise: Data curation, Formal analysis, Investigation, Methodology, Software, Validation, Visualization, Writing – original draft. **Fritz Schick:** Supervision, Writing – review & editing. **Norbert Stefan:** Resources, Writing – review & editing. **Jürgen Machann:** Conceptualization, Investigation, Methodology, Project administration, Resources, Funding acquisition, Writing – review & editing.

Declaration of competing interest

The authors declare that they have no known competing financial interests or personal relationships that could have appeared to influence the work reported in this paper.

Acknowledgements

We thank all participants who took part in the studies and the staff in this research program. Additionally, we thank Stephan Kannengießer from Siemens Healthineers for his valuable support.

References

[1] I.J. Neeland, R. Ross, J.-P. Després, et al., Visceral and ectopic fat, atherosclerosis, and cardiometabolic disease: a position statement, Lancet Diabetes Endocrinol. 7 (2019) 715–725, https://doi.org/10.1016/S2213-8587(19)30084-1.

[2] C. Falank, H. Fairfield, M.R. Reagan, Signaling interplay between bone marrow adipose tissue and multiple myeloma cells, Front. Endocrinol. 7 (2016) 67, https://doi.org/10.3389/fendo.2016.00067.

[3] K.M. Beekman, G. Duque, A. Corsi, et al., Osteoporosis and bone marrow adipose tissue, Curr. Osteoporos. Rep. 21 (2023) 45–55, https://doi.org/10.1007/s11914-022-00768-1.

[4] K.A. Britton, C.S. Fox, Ectopic fat depots and cardiovascular disease, Circulation 124 (2011), https://doi.org/10.1161/CIRCULATIONAHA.111.077602.

[5] N. Aaron, S. Costa, C.J. Rosen, L. Qiang, The implications of bone marrow adipose tissue on inflammaging, Front. Endocrinol. 13 (2022) 853765, https://doi.org/10.3389/fendo.2022.853765.

[6] N. Stefan, A. Fritsche, F. Schick, H.-U. Häring, Phenotypes of prediabetes and stratification of cardiometabolic risk, Lancet Diabetes Endocrinol. 4 (2016) 789–798, https://doi.org/10.1016/S2213-8587(16)00082-6.

[7] B.H. Goodpaster, B.C. Bergman, A.M. Brennan, L.M. Sparks, Intermuscular adipose tissue in metabolic disease, Nat. Rev. Endocrinol. 19 (2023) 285–298, https://doi.org/10.1038/s41574-022-00784-2.

[8] M. Borga, J. West, J.D. Bell, et al., Advanced body composition assessment: from body mass index to body composition profiling, J. Investig. Med. off Publ. Am. Fed. Clin. Res. 66 (2018) 1–9, https://doi.org/10.1136/jim-2018-000722.

[9] T. Haueise, F. Schick, N. Stefan, et al., Analysis of volume and topography of adipose tissue in the trunk: results of MRI of 11,141 participants in the German National Cohort, Sci. Adv. 9 (2023) eadd0433, https://doi.org/10.1126/sciadv.add0433.

[10] J. Machann, M. Hasenbalg, J. Dienes, et al., Short-term variability of proton density fat fraction in pancreas and liver assessed by multiecho chemical-shift encoding-based MRI at 3 T, J. Magn. Reson. Imaging JMRI (2022), https://doi.org/10.1002/jmri.28084.

[11] J. Machann, C. Thamer, B. Schnoedt, et al., Hepatic lipid accumulation in healthy subjects: a comparative study using spectral fat-selective MRI and volume-localized1H-MR spectroscopy, Magn. Reson. Med. 55 (2006) 913–917, https://doi.org/10.1002/mrm.20825.

[12] L.S. Kiefer, J. Fabian, S. Rospleszcz, et al., Assessment of the degree of abdominal myosteatosis by magnetic resonance imaging in subjects with diabetes, prediabetes and healthy controls from the general population, Eur. J. Radiol. 105 (2018) 261–268, https://doi.org/10.1016/j.ejrad.2018.06.023.

[13] H. Eggers, P. Börnert, Chemical shift encoding-based water-fat separation methods, J. Magn. Reson. Imaging JMRI 40 (2014) 251–268, https://doi.org/10.1002/jmri.24568.

[14] X. Zhong, M.D. Nickel, S.A.R. Kannengiesser, et al., Liver fat quantification using a multi-step adaptive fitting approach with multi-echo GRE imaging, Magn. Reson. Med. 72 (2014) 1353–1365, https://doi.org/10.1002/mrm.25054.

[15] H.H. Hu, T. Yokoo, M.R. Bashir, et al., Linearity and bias of proton density fat fraction as a quantitative imaging biomarker: a multicenter, multiplatform, multivendor phantom study, Radiology 298 (2021) 640–651, https://doi.org/10.1148/radiol.2021202912.

[16] T. Hayashi, K. Fukuzawa, H. Yamazaki, et al., Multicenter, multivendor phantom study to validate proton density fat fraction and T2* values calculated using vendor-provided 6-point DIXON methods, Clin. Imaging 51 (2018) 38–42, https://doi.org/10.1016/j.clinimag.2018.01.011.

[17] J.K. Jang, S.S. Lee, B. Kim, et al., Agreement and reproducibility of proton density fat fraction measurements using commercial MR sequences across different platforms: a multivendor, multi-institutional phantom experiment, Invest. Radiol. 54 (2019) 517–523, https://doi.org/10.1097/RLI.0000000000000561.

[18] T. Yokoo, S.D. Serai, A. Pirasteh, et al., Linearity, Bias, and precision of hepatic proton density fat fraction measurements by using MR imaging: a meta-analysis, Radiology 286 (2018) 486–498, https://doi.org/10.1148/radiol.2017170550.

[19] C. Zhan, S. Olsen, H.C. Zhang, et al., Detection of hepatic steatosis and iron content at 3 Tesla: comparison of two-point Dixon, quantitative multi-echo Dixon, and MR spectroscopy, Abdom. Radiol. NY 44 (2019) 3040–3048, https://doi.org/10.1007/s00261-019-02118-9.

[20] J. Starekova, D. Hernando, P.J. Pickhardt, S.B. Reeder, Quantification of liver fat content with CT and MRI: state of the art, Radiology 301 (2021) 250–262, https://doi.org/10.1148/radiol.2021204288.

[21] J. Burakiewicz, C.D.J. Sinclair, D. Fischer, et al., Quantifying fat replacement of muscle by quantitative MRI in muscular dystrophy, J. Neurol. 264 (2017) 2053–2067, https://doi.org/10.1007/s00415-017-8547-3.

[22] K. Engelke, O. Chaudry, L. Gast, et al., Magnetic resonance imaging techniques for the quantitative analysis of skeletal muscle: State of the art, J. Orthop. Transl. 42 (2023) 57–72, https://doi.org/10.1016/j.jot.2023.07.005.

[23] K.J. Suchacki, A.A.S. Tavares, D. Mattiucci, et al., Bone marrow adipose tissue is a unique adipose subtype with distinct roles in glucose homeostasis, Nat. Commun. 11 (2020) 3097, https://doi.org/10.1038/s41467-020-16878-2.

[24] C. Le Ster, G. Gambarota, J. Lasbleiz, et al., Breath-hold MR measurements of fat fraction, T1, and T2 * of water and fat in vertebral bone marrow, J. Magn. Reson. Imaging JMRI 44 (2016) 549–555, https://doi.org/10.1002/jmri.25205.

[25] J. Machann, N. Stefan, F. Schick, (1)H MR spectroscopy of skeletal muscle, liver and bone marrow, Eur. J. Radiol. 67 (2008) 275–284, https://doi.org/10.1016/j.ejrad.2008.02.032.

[26] D. Hasic, R. Lorbeer, R.C. Bertheau, et al., Vertebral bone marrow fat is independently associated to VAT but not to SAT: KORA FF4—whole-body MR imaging in a population-based cohort, Nutrients 12 (2020) 1527, https://doi.org/10.3390/nu12051527.

[27] Y. Leonhardt, F.T. Gassert, G. Feuerriegel, et al., Vertebral bone marrow T2* mapping using chemical shift encoding-based water-fat separation in the quantitative analysis of lumbar osteoporosis and osteoporotic fractures, Quant. Imaging Med. Surg. 11 (2021) 3715–3725, https://doi.org/10.21037/qims-20-1373.

[28] M. Jung, S. Rospleszcz, M.T. Löffler, et al., Association of lumbar vertebral bone marrow and paraspinal muscle fat composition with intervertebral disc degeneration: 3T quantitative MRI findings from the population-based KORA study, Eur. Radiol. 33 (2023) 1501–1512, https://doi.org/10.1007/s00330-022-09140-4.

[29] T. Kart, M. Fischer, T. Küstner, et al., Deep learning-based automated abdominal organ segmentation in the UK biobank and german national cohort magnetic resonance imaging studies, Invest. Radiol. 56 (2021) 401, https://doi.org/10.1097/RLI.0000000000000755.

[30] T. Haueise, N. Stefan, T.J. Schulz, et al., Automated shape-independent assessment of the spatial distribution of proton density fat fraction in vertebral bone marrow, Z Für Med. Phys. (2023), https://doi.org/10.1016/j.zemedi.2022.12.004.

[31] H. Yamazaki, S. Tauchi, J. Machann, et al., Fat distribution patterns and future type 2 diabetes, Diabetes 71 (2022) 1937–1945, https://doi.org/10.2337/db22-0315.

[32] J.Z. Bojorquez, S. Bricq, C. Acquitter, et al., What are normal relaxation times of tissues at 3 T? Magn. Reson. Imaging 35 (2017) 69–80, https://doi.org/10.1016/j.mri.2016.08.021.

[33] C.M.J. de Bazelaire, G.D. Duhamel, N.M. Rofsky, D.C. Alsop, MR imaging relaxation times of abdominal and pelvic tissues measured in vivo at 3.0 T: preliminary results, Radiology 230 (2004) 652–659, https://doi.org/10.1148/radiol.2303021331.

[34] F. Schick, H. Bongers, W.I. Jung, et al., Volume-selective proton MRS in vertebral bodies, Magn. Reson. Med. 26 (1992) 207–217, https://doi.org/10.1002/mrm.1910260203.

[35] F. Bamberg, H.-U. Kauczor, S. Weckbach, et al., Whole-body MR imaging in the German national cohort: rationale, design, and technical background, Radiology 277 (2015) 206–220, https://doi.org/10.1148/radiol.2015142272.

[36] F. Bamberg, H. Hetterich, S. Rospleszcz, et al., Subclinical disease burden as assessed by whole-body MRI in subjects with prediabetes, subjects with diabetes, and normal control subjects from the general population: the KORA-MRI study, Diabetes 66 (2017) 158–169, https://doi.org/10.2337/db16-0630.

[37] R.C. Bertheau, R. Lorbeer, J. Nattenmüller, et al., Bone marrow fat fraction assessment in regard to physical activity: KORA FF4–3-T MR imaging in a population-based cohort, Eur. Radiol. 30 (2020) 3417–3428, https://doi.org/10.1007/s00330-019-06612-y.

[38] D.C. Karampinos, S. Ruschke, M. Dieckmeyer, et al., Quantitative MRI and spectroscopy of bone marrow, J. Magn. Reson. Imaging JMRI 47 (2018) 332–353, https://doi.org/10.1002/jmri.25769.

[39] M.A. Bredella, M. Torriani, R.H. Ghomi, et al., Vertebral bone marrow fat is positively associated with visceral fat and inversely associated with IGF-1 in obese women, Obes. Silver Spring Md. 19 (2011) 49–53, https://doi.org/10.1038/oby.2010.106.

[40] F. Schick, H. Einsele, B. Weiß, et al., Assessment of the composition of bone marrow prior to and following autologous BMT and PBSCT by magnetic resonance, Ann. Hematol. 72 (1996) 361–370, https://doi.org/10.1007/s002770050187.

[41] T.J. Littlejohns, J. Holliday, L.M. Gibson, et al., The UK Biobank imaging enhancement of 100,000 participants: rationale, data collection, management and future directions, Nat. Commun. 11 (2020) 2624, https://doi.org/10.1038/s41467-020-15948-9.

[42] D.E. Horng, D. Hernando, S.B. Reeder, Quantification of liver fat in the presence of iron overload, J. Magn. Reson. Imaging JMRI 45 (2017) 428–439, https://doi.org/10.1002/jmri.25382.

[43] H. Wang, Y. Leng, Y. Gong, Bone marrow fat and hematopoiesis, Front. Endocrinol. 9 (2018) 694, https://doi.org/10.3389/fendo.2018.00694.